A Mechano-Regulation Model of Fracture Repair in Vertebral Bodies

A. Boccaccio[1], D.J. Kelly[2*], C. Pappalettere[1]

[1]*Dipartimento di Ingegneria Meccanica e Gestionale, Politecnico di Bari, 70126, Bari, Italy*

[2] *Trinity Centre for Bioengineering, School of Engineering, Trinity College Dublin, Ireland.*

*Corresponding author:

Dr. Daniel Kelly

Mailing Address:

Centre for Bioengineering,

Department of Mechanical Engineering,

Trinity College Dublin,

Dublin 2,

Ireland.

Contact Information:

Tel: +353-1-6083947 (Daniel Kelly);

Fax: +353-1-6795554 (Daniel Kelly);

Email: kellyd9@tcd.ie (Daniel Kelly);

Keywords: Mechanobiology; Fracture Repair; Vertebral Body; Tissue differentiation; Finite element analysis.

Running title: Mechanobiology of fracture repair

ABSTRACT

In this study a multi-scale mechano-regulation model was developed in order to investigate the mechanobiology of trabecular fracture healing in vertebral bodies. A macro-scale finite element model of the spinal segment L3-L4-L5, including a mild wedge fracture in the body of the L4 vertebra, was used to determine the boundary conditions acting on a micro-scale finite element model simulating a portion of fractured trabecular bone. The micro-scale model, in turn, was utilized to predict the local patterns of tissue differentiation within the fracture gap and then how the equivalent mechanical properties of the macro-scale model change with time. The patterns of tissue differentiation predicted by the model appeared consistent with those observed *in vivo*. Bone formation occurred primarily through endochondral ossification. New woven bone was predicted to occupy the majority of the space within the fracture site approximately 7-8 weeks after the fracture event. Remodeling of cancellous bone architecture was then predicted, with complete new trabeculae forming due to bridging of the microcallus between the remnant trabeculae.

1. INTRODUCTION

Vertebral fractures commonly occur in elderly people with osteoporosis.[1] For example, in the United States vertebral fractures account for nearly half of all osteoporotic fractures.[1] With age the structure of cancellous bone within vertebral bodies transforms from that characterized by predominantly plate-like trabeculae to rod-like trabeculae.[2] This change leads to an age-related decrease in trabecular bone mass.[2] The reduced bone mass observed in vertebral bodies, particularly with osteoporosis, is generally accompanied by greater amounts of microcallus formations around injured trabeculae.[2,3] This weakening of the tissue means that spine fractures may occur after minimal trauma.[4-6] While the cascade of events that occur during fracture healing of long bones has been well characterized[7,8], there is less reported on the natural healing process that occurs following acute fracture of a vertebral body.[9-11] It has been suggested that the stabilization of a fracture of the vertebrae is mainly a process of the cancellous bone rather than a process of the cortex, with fractured vertebrae presenting the same morphology of callus as described for microcallus formations.[2]

Fracture healing in long bones normally follows an orderly process[7], with healing occurring by a process that involves both intramembraous and endochondral ossification. Mechanical factors are known to play a key role in such bone healing.[12,13] Numerous previous studies have used computational models to investigate the role of biophysical stimuli in regulating the tissue differentiation process during fracture healing of long bones.[14-19] More recently such mechano-regulation models have been extended to include factors such as random-walk algorithms of cell dispersal[20], cell-phenotype specific activity[21] and angiogenesis[22] which provides further support for the role of mechanical factors in regulating the events that occur during fracture repair. There is also evidence to suggest that the same mechanobiological principles that regulate diaphyseal fracture healing also influence bone formation and remodeling during trabecular bone fracture healing.[23] By utilizing fuzzy logic rules in combination with a finite element model, it was possible to predict repair through the formation of woven bone in the fracture site and eventually the formation of a trabecular structure[23], representative of the events that occur during fracture repair in the metaphyseal and epiphyseal regions of long bones.

Only recently have the stages of fracture healing in acute human osteoporotic vertebral body fractures been characterized by histomorphometric analysis.[11] Four stages of fracture healing were identified in biopsy specimens: (i) fracture haematoma, (ii) chondrogenesis and bone matrix synthesis, (iii) endochondral ossification and woven bone formation, and (iv) bone modeling and remodeling.

The objective of this study was to investigate if biophysical stimuli play a role in regulating this process. To determine the magnitude of such stimuli at the level of individual trabeculae, a multi-scale finite element approach was adopted. A number of previous studies have used multi-scale modeling approaches in biomechanics and mechanobiology, for example to model complex mechanisms occurring in various cells [24,25], in cartilage[26], bone[27,28] and in scaffolds for bone regeneration.[29,30] Our hypothesis was that a mechano-regulation model for tissue differentiation[31] that has previously been used to predict the time-course of fracture repair in long bones[14] can be used to predict trabecular bone healing in fractured vertebrae at the level of individual trabeculae.

2. METHODS

2.1 Macro-scale model of spinal segment

Two finite element models of the spinal segment L3-L4-L5 were created (Fig. 1), building on a previous model.[32] The first (Fig. 1(A)) included the body of a healthy L4 vertebra, in the second one the same vertebra was modelled as fractured (Fig. 1(B)). The healthy model was used to help corroborate the finite element model of the spinal segment, whereas, the model with the fractured vertebra was utilized to predict the patterns of tissue differentiation occurring during the fracture healing. The finite element code ABAQUS (Hibbit et al., Rhode Island, USA) was utilized. CT scan data (slice thickness 3 mm, pixel size 0.9 mm, Toshiba Inc.) of a 52 years old male subject were utilized for the generation of the mesh of the entire L3 and L5 vertebrae and the posterior processes of the L4 vertebra. An idealised model of the L4 as well as the intervertebral discs located above and below was developed. In the healthy model, the L4 vertebra had a constant height (Fig. 1(C)) whereas in the fractured one the vertebral height decreased by 20% from the posterior processes towards the anterior side (Fig. 1(D)-(E)). In the Genant grading[33], such a fracture is classified as a mild wedge fracture. Full details of the macro-scale finite element model are available online as Supplementary Material A.

2.2 Micro-scale model of trabecular bone

The micro-scale model of the trabecular bone was similar in geometry to that used by Shefelbine et al.[23] (Fig. 2). A diastasis of 0.5 mm was simulated, with the trabeculae bordering the gap idealized as prismatic domains 0.1 mm thick. The space between fractured trabeculae was hypothesized to be occupied by granulation tissue. Both the trabecular bone and the granulation tissue were modelled as biphasic poroelastic materials. Table 1 lists the mechanical properties utilized for the micro-scale model.

Following the fracture event the granulation tissue was gradually replaced by repair tissue according to the rules of the algorithm described below (Section 2.3). The value of the Young's modulus for the mature bone in the micro-scale model was set equal to 1440 MPa. This value was chosen based on the fact that the transversal area occupied by the trabeculae spicules was 1/4 of the total transversal area, yielding an equivalent Young's modulus along the vertical direction of 360 MPa, which was the assumed value of the

equivalent Young's modulus for the cancellous bone along the vertical direction z in the macro-scale model (see Table SMA1 reported in the Supplementary Material A). Similar values have been used in the literature.[38]

For both the micro and the macro-scale model, poroelastic elements available in ABAQUS (C3D8P, 8 node trilinear displacement and pore pressure; 8 gauss points) have been used.

2.3 Multi-scale mechano-regulation model of tissue differentiation

A multi-scale approach was adopted. The macro-scale model of the spinal segment was utilized to determine the elastic and poroelastic boundary conditions acting on eight different micro-scale models which were hypothesized to represent different regions in the fractured cancellous bone situated in the neighbourhood of the points $P_1,\ldots,P_8$ (Fig. 3). The micro-scale model, in turn, was utilized to predict the local patterns of tissues differentiation during the fracture repair process and how the equivalent mechanical properties of the macro-scale model change with time. The equations describing tissue differentiation were implemented into an algorithm, a graphical summary of which is depicted in Fig. 4. The time period investigated corresponded to the first 100 days after the fracture event. The equivalent mechanical properties for the fractured region of the macro-scale model were first determined (Block [1]). To this end, a strain ε_{imp}=5 % was imposed by applying a displacement $\delta=\varepsilon_{imp}\cdot L_{\mu s}$ ($L_{\mu s}$=0.7 mm being the height of the micro-scale model) to the top surface of the micro-scale model, and based on the value of the reaction force F at the constraints (placed on the bottom surface) preventing vertical translation, an equivalent Young's modulus for the macro-scale model E_{equiv_ms} was determined as:

$$E_{equiv\_ms} = \frac{F \cdot L_{\mu s}}{A \cdot \delta} \quad (1)$$

where, A=0.6·0.6 mm^2 was the transverse area of the micro-scale model. The displacement was applied over a time period of 1000 seconds. Preliminary tests demonstrated that for such a long time period the drained condition was reached and hence the bone callus, which was modeled as a biphasic poroelastic material, behaved as an elastic one. Concerning the other mechanical properties (e.g. Poisson's ratio, Bulk modulus, etc), their equivalent value for the macro-scale model was computed as the average of the values of the mechanical properties of each element making up the micro-scale model. These equivalent mechanical

properties were inputted into the macro-scale model (Block [2]) and then a first FE analysis was performed on the spinal segment (Block [3]).

An axial compression of 1000 N was applied to the centre of mass of the L3 vertebra and ramped over a time period of 1 s (which can be considered the time in which a subject assumes the erect position). This load was applied for each iteration (day) of the 100 days investigated. A group of about 10 elements situated in the neighborhood of each point $P_1,\ldots,P_8$ within the macro-scale model was considered; for each group, the average value of strain in the vertical direction ε_{zzPi}, and pore pressure p_{pore} were determined (Block [4]). Next, a compression test was simulated (Block [5], Block [6]) on the micro-scale model. The inferior surface was constrained and a vertical displacement ΔL_{Pi} was applied on the top surface given by:

$$\Delta L_{Pi}=\varepsilon_{zzPi}\cdot L_{\mu s} \tag{2}$$

The pore pressure averaged from the neighbourhood of each point $P_1,\ldots,P_8$, was applied on the six external faces of each of the eight micro-scale models. The compression load and pore pressure were ramped over a time period of 1 s. Based on the values of strain and fluid flow velocity predicted in each element of the fracture site domain, the biophysical stimulus S was determined (Block [7]). Specifically, if γ is the octahedral shear strain and v is the fluid flow velocity, the stimulus S was determined using:

$$S=\frac{\gamma}{a}+\frac{v}{b} \tag{3}$$

a=3.75% and b=3μms^{-1} being empirical constants.[39] The new tissue phenotype was then determined (Block [8], Block [9]):

$$if\quad\begin{cases} S>m\Rightarrow fibroblast: \quad fibrous\quad connective\quad tissue \\ 1<S<m\Rightarrow chondrocyte: \quad cartilage \\ n_{resorbtion}<S<1\Rightarrow osteoblast: \quad mature\quad woven\quad bone \\ 0<S<n_{resorbtion}\Rightarrow osteoclast: \quad bone\quad resorbtion \end{cases} \tag{4}$$

where $n_{\text{resorption}}$=0.01, and m=3 represent boundaries of the mechano-regulation diagram for tissue differentiation.[14]

A diffusion analysis was performed for the micro-scale model to simulate the process of mesenchymal stem cell (MSC) migration through the space between the trabeculae. If c is the concentration of the MSCs in a given volume and D is the diffusion coefficient, the dispersal of MSCs can be described as:

$$\frac{\mathbf{d}c}{\mathbf{d}t} = D\nabla^2 c \tag{5}$$

The parameter of Eqn. (5) (i.e. the D diffusion coefficient) was set so that the complete cell coverage of the space between the trabeculae was achieved two days after the fracture event. The elastic modulus of the differentiating tissues was then estimated according to an exponential law developed previously.[40,41] Finally, the algorithm incorporated a simple rule of mixtures described in Lacroix and Prendergast[14] (Block [10]). Further details of the exponential law and of the rule of mixtures implemented in the algorithm are available online as Supplementary Material B.

A third finite element analysis was performed (Block [11]), simulating a compression test of the micro-scale geometry to determine the equivalent elastic modulus to be inputted in the next iteration in the macro-scale model (Block [12]). The pore pressure boundary condition determined from the macro-scale model was removed from the micro-scale model for this analysis (i.e. p_{pore}=0). In other words, this analysis simulated the drained condition of a poroelastic material where the pore pressure p_{pore}=0 and the structural response is dependant only on the ground substance while the effect of the liquid phase is negligible. A displacement δ producing an average strain of ε_{imp}=5% (δ=$\varepsilon_{imp}\cdot L_{\mu s}$) was applied on the top surface of the prismatic domain, ramped over a time period of 1000 s; the inferior surface was hypothesized to be constrained. Equivalent mechanical properties were determined for each of the eight micro-scale models associated with the points P_1,…,P_8. Knowing the reaction force F at the constraints, an equivalent Young's modulus was determined according to Eqn. (1). It was assumed that the spatial changes in the mechanical properties in the macro-scale model could be described with a cubic interpolation law (Block [13]). Given that only an axial load was applied to the centre of mass of the L3 vertebra, it was assumed that the distribution of the mechanical properties within the vertebral fracture was symmetric with respect to the axis connecting the points P_2 and P_3 and does not change with respect to z (Fig. 3). The variability of the mechanical properties in the plane (x,y) was modelled by means of the user defined FORTRAN subroutine

UFIELD available in ABAQUS. The equation describing the change in space of the mechanical properties was of the form:

$$MP=Ax^3+By^3+Cx^2y+Dxy^2+Exy+Fx+Gy+H \quad (6)$$

where *MP* was the mechanical property under consideration (e.g Young's modulus, permeability etc), *x* and *y* are the plane coordinates (Fig. 3). *A*, *B*, …. *H* are coefficients computed in each cycle of the algorithm that regulate the shape of the cubic surface *MP=MP(x,y)*.

RESULTS

The Von Mises stress distribution predicted by the spinal segment model in the first day after the fracture event was quite symmetrical with respect to the middle sagittal plane and reached a maximum value at the point where the fracture gap had the greatest thickness (Fig. 5(A)). In the unfractured model the compression load produced a vertical displacement with very small relative rotations between the vertebrae (Fig. 5(B)). The magnitude of these rotations became significant in the fractured model where, due to the shape of the wedge fracture, the centre of gravity of the L3 vertebra moved anteriorly (Fig. 5(C)).

The space between the fractured trabeculae was predicted to be mostly occupied by fibrous tissue in the initial days after the fracture event (see Fig. 6 that demonstrates the patterns predicted for the points P_1, P_2 and P_3). During the first 30-35 days after the fracture event the amount of fibrous tissue predicted decreased significantly and disappeared completely after six weeks. Small amounts of cartilage appeared during the first week, and approximately 40% of the space between the fractured trabeculae was occupied by cartilage after one month. This cartilaginous tissue was completely replaced by bone after two months. Small amounts of bone were predicted to form after the first two weeks and after the second month the space was entirely occupied by bone. Bone deposition was predicted to initiate at the fractured trabecular ends. The bone remodeling process was initiated after the second month and reached an equilibrium at the end of the third month. The remodeled trabeculae were aligned with those bordering the fractured region.

Small differences were predicted between the patterns of bony tissue formed the points P_1, P_2 and P_3 (Fig. 7). In particular it appeared that the bone re-growth process occurred more slowly at the point P_2. For

example, after 56 days bone was predicted to completely occupy the space between the trabeculae for the point P_3, whereas for the points P_1 and P_2 some small regions were still occupied by other tissues. However, in general the predicted patterns of trabecular bone repair were similar at all points within the fracture gap.

Bone initially formed at the fractured trabecular ends, replacing a cartilaginous template through the process of endochondral bone formation. There was a near linear increase in the amount of bone tissue within the callus during the first 60 days of repair (Fig. 8). Bone resorption led to rapid reorganization of the repair tissue, with near ideal levels of bone remaining at equilibrium at each point in the fracture gap.

DISCUSSION

This paper presented a multi-scale model of vertebral fracture repair, where a multi-scale finite element model of a spinal segment was used to predict the magnitude of various biophysical stimuli acting in the callus surrounding regenerating trabeculae. The displacement field (Fig. 5) predicted by the macro-scale model was rather consistent with the results reported by Rohlmann et al.[42], who found that a wedge-shaped fracture of a vertebral body increases the flexion bending moment due to the upper body weight. The spatial and temporal patterns of tissue differentiation predicted by this model are also in general agreement with that observed experimentally[11], providing further evidence that certain biophysical stimuli regulate tissue differentiation in a similar manner in diaphyseal fractures and in trabecular bone fractures in the vertebrae. Diamond et al.[11] describe 4 stages of fracture healing process in the vertebral body, with significant overlap between the various stages of healing. Chondrogenesis was evident in the second stage of the fracture healing process, which followed the initial granulation tissue stage (characterized by necrotic bone and fibrovascular stroma). The appearance of cartilaginous tissue in the days following the fracture event was also predicted by the model (Figs. 6 and 8). This cartilaginous tissue was predicted to be gradually replaced by woven bone. Such endochondral ossification has also been observed in experimental studies (stage 3).[9-11] The model then predicted a peak in bone formation (Figs. 7-8). Hyperosteoidosis/Osteosclerosis (excessive formation of osteoid) has also been observed experimentally at comparable time-points.[11] New woven bone can occupy most of the marrow space during this stage, a phenomena also predicted by the model (Fig. 7).

Finally remodeling of the cancellous bone architecture was predicted. Complete new trabeculae are predicted to form due to bridging of the microcallus between the remnant trabeculae, leading to restructuring of the bone architecture.[2]

A feature of vertebral fractures is the overlap between the different stages of healing within a given body, with two or more stages of fracture healing in the same biopsy specimen.[11] No large differences were observed in the predicted temporal patterns of tissue differentiation at different points in the vertebral body, which would appear to be at odds with the experimental observations of overlap. It has been suggested that in vertebral bodies the fracture stabilization that permits orderly repair in long bones is not possible due to repetitive injury. A limitation of the present model is that the mechano-regulation algorithm does not include a damaged tissue region that would allow tissue to fracture and new callus to form in regions experiencing high levels of biophysical stimulation (e.g. strain). Therefore this study has only considered the original injury event. A 'tissue destruction' phase[23] will be included in future mechano-regulation models. In addition, more consideration of osteoclastic and osteoblast activity[43], and associated trabecular microdamage[44,45], may ultimately lead to models that can predict the modeling, remodeling, fracture and repair of trabecular bone. Regardless, the predictions of the present model suggest that experimental observations of significant overlap between the various stages of healing[11] are due to multiple fracture events initiated at different times.

There are other limitations of the presented model. It was assumed that viable granulation tissue/bone marrow completely fills the volume between fractured vertebrae following the fracture event. A simplified cancellous bone geometry was assumed, but more accurate micro-scale geometries could be considered, as has been implemented for mechano-regulation models within irregular scaffolds.[46] Another limitation was that in each iteration only one loading cycle is applied on the spinal segment, which was assumed to be representative of the typical loading experienced during a given day. Similar assumptions are adopted in previous studies.[14,47,48] In patients with vertebral fractures, vertebrae can undergo to more complex loading cycles and the frequency of the loading cycles is patient specific. The utilization of a multi-scale approach presents its own unique problems for mechanobiological models. For example, up-scaling of

material properties from the micro-scale to the macro-scale was only based on only 8 micro-scale models within the callus, with a cubic interpolation function used to estimate material properties in intermediate regions. Therefore spatial variation in mechanical properties was greatly simplified. Also, the fracture gap was modeled as heterogeneous isotropic in the macro-scale model; ideally this region should be modeled as heterogeneous and transversely isotropic (i.e. the same modeling assumption as utilized for the cancellous bone within the L4 vertebra). In the present model, due to the intrinsic limitation of the adopted micro-scale model (that includes only vertical trabeculae with no trabeculae lying on the horizontal plane), only isotropic material properties are computed when up-scaling from the micro-scale model to the macro-scale model. The elastic properties in the other directions (1 or 2, see Fig. 2) should be determined by simulating compression tests in these directions; however the absence of trabeculae lying on the horizontal plane would lead to incorrect predictions of the elastic moduli. Increases in computational power will ultimately allow better micro-scale models to be developed to more accurately simulate the geometric complexity of the regenerating fracture gap and will allow more "physiologic" loading conditions acting on the lumbar vertebrae during the healing period to be considered. Other factors known to partially regulate fracture healing, such as angiogenesis[22,49] and growth factors,[50,51] were also not included in the model.

In conclusion, this paper presented a multi-scale approach to investigate the mechanobiology of trabecular fracture healing. The predictions of the model suggest that trabecular fracture healing in vertebral bodies is similarly mechano-regulated to diaphyseal fracture healing. The study used a mechano-regulation hypothesis first proposed by Prendergast et al.[31], and the same model parameters as has been used in numerous other predictions of tissue repair including long-bone fracture healing[14,52,53]. These mechanobiological models must be continually tested to assess if they can predict the sequence of events that occur during other reparative events that occur in the body, [40, 47] in order to provide further corroboration for the hypotheses on which the models are based. Future tests of the underlying modeling hypotheses should also include investigating if the same model parameters can be used to predict vertebral fracture repair under altered loading conditions. This will provide greater confidence that such models can be used to improve physical rehabilitation regimes or the design of orthopedic devices. For example, it may be possible to

predict how gradual increases in loading in the days following a fracture event will influence the healing outcome. Furthermore, the proposed modeling framework could be extended to help optimize new regenerative medicine approaches to repairing normal tissue bone architecture following trauma or disease.

ACKNOWLEDGEMENTS

Dr. Kelly is funded by Science Foundation Ireland under the President of Ireland Young Researcher Award (08/YI5/B1336).

REFERENCES

1. Cummings S, Melton Iii LJ. 2002. Epidemiology and outcomes of osteoporotic fractures. Lancet 359:1761-1767.
2. Amling M, Pösl M, Ritzel H, et al. 1996. Architecture and distribution of cancellous bone yield vertebral fracture clues. A histomorphometric analysis of the complete spinal column from 40 autopsy specimens. Arch Orthop Trauma Surg 115:262-269.
3. Hansson T, Roos B. 1981. Microcalluses of the trabeculae in lumbar vertebrae and their relation to the bone mineral content. Spine 6:375-380.
4. Antonacci MD, Hanson DS, Leblanc A, et al. 1997. Regional variation in vertebral bone density and trabecular architecture are influenced by osteoarthritic change and osteoporosis. Spine 22:2393-2402.
5. Eastell R, Cedel SL, Wahner HW, et al. 1991. Classification of vertebral fractures. J Bone Miner Res 6:207-215.
6. Heggeness MH. 1993. Spine fracture with neurological deficit in osteoporosis. Osteoporos Int 3:215-221.
7. Einhorn TA. 2005. The science of fracture healing. J Orthop Trauma, 19(10 SUPPL.):S4-S6.
8. Gerstenfeld LC, Cullinane DM, Barnes GL, et al. 2003. Fracture healing as a post-natal developmental process: Molecular, spatial, and temporal aspects of its regulation. J Cell Biochem 88:873-884.
9. Antonacci MD, Mody DR, Rutz K, et al. 2002. A histologic study of fractured human vertebral bodies. J Spinal Disord 15:118-126.
10. Togawa D, Lieberman IH, Bauer TW, et al. 2005. Histological evaluation of biopsies obtained from vertebral compression fractures: Unsuspected myeloma and osteomalacia. Spine 30:781-786.

11. Diamond TH, Clark WA, Kumar SV. 2007. Histomorphometric analysis of fracture healing cascade in acute osteoporotic vertebral body fractures. Bone 40:775-780.

12. Pauwels, F. 1980. Eine neue theorie über den einfluβ mechanischer reize auf die differenzierung der stützgewebe. Z Anat Entwickl. Gesch. 121, 478-515. Translated as A new theory concerning the influence of mechanical stimuli on the differentiation of the supporting tissues. In: Maquet, P., Furlong, R., (Eds) Biomechanics of the Locomotor apparatus, Springer, Berlin, 375-407.

13. Claes LE, Heigele CA, Neidlinger-Wilke C, et al. 1998. Effects of mechanical factors on the fracture healing process. Clin Orthop Relat Res (355 SUPPL.):S132-S147.

14. Lacroix D, Prendergast PJ. 2002. A mechano-regulation model for tissue differentiation during fracture healing: Analysis of gap size and loading. J Biomech 35:1163-1171.

15. Carter DR, Blenman PR, Beaupré GS. 1988. Correlations between mechanical stress history and tissue differentiation in initial fracture healing. J Orthop Res 6:736-748.

16. Claes LE, Heigele CA. 1999. Magnitudes of local stress and strain along bony surfaces predict the course and type of fracture healing. J Biomech 32:255-266.

17. Isaksson H, van Donkellar CC, Huiskes R, et al. 2006. Corroboration of mechanoregulatory algorithms for tissue differentiation during fracture healing: Comparison with in vivo results. J Orthop Res 24:898-907.

18. Gòmez-Benito MJ, Garcìa-Aznar JM, Kuiper JH, et al. 2005. Influence of fracture gap size on the pattern of long bone healing: A computational study. J Theor Biol 235:105-119.

19. Andreykiv A, Van Keulen F, Prendergast PJ. 2008. Simulation of fracture healing incorporating mechanoregulation of tissue differentiation and dispersal/proliferation of cells. Biomech Model Mechanobiol 7:443-461.

20. Pérez MA, Prendergast PJ. 2007. Random-walk models of cell dispersal included in mechanobiological simulations of tissue differentiation. J Biomech 40:2244-2253.

21. Isaksson H, van Donkelaar CC, Huiskes R, et al. 2008. A mechano-regulatory bone-healing model incorporating cell-phenotype specific activity. J Theor Biol 252:230-246.

22. Checa S, Prendergast PJ. 2009. A mechanobiological model for tissue differentiation that includes angiogenesis: A lattice-based modeling approach. Ann Biomed Eng 37:129-145.

23. Shefelbine SJ, Augat P, Claes L, et al. 2005. Trabecular bone fracture healing simulation with finite element analysis and fuzzy logic. J Biomech 38:2440-2450.

24. Sanz-Herrera JA, Moreo P, García-Aznar JM, et al. 2009. On the effect of substrate curvature on cell mechanics. Biomaterials 30, 6674-6686.

25. Lavagnino M, Arnoczky SP, Kepich E, et al. 2008. A finite element model predicts the mechanotransduction response of tendon cells to cyclic tensile loading. Biomech Model Mechanobiol 7:405-416.

26. Guilak F, Mow VC. 2000. The mechanical environment of the chondrocyte: a biphasic finite element model of cell-matrix interactions in articular cartilage. J Biomech 33:1663-1673.

27. Beilin V, Pande GN, Ito K. 2000. Numerical simulation of the influence of rough bone-callus interface on the healing of fractured bone. Mechanics of Composite Materials 36:373-378.

28. Ilic S, Hackl K, Gilbert R. 2010. Application of the multiscale FEM to the modeling of the cancellous bone. Biomech Model Mechanobiol 9:87-102.

29. Jungreuthmayer C, Jaasma MJ, Al-Munajjed AA, et al. 2009. Deformation simulation of cells seeded on a collagen-GAG scaffold in a flow perfusion bioreactor using a sequential 3D CFD-elastostatics model. Med Eng Phys 31:420-427.

30. Sanz-Herrera JA, García-Aznar JM, Doblaré M. 2008. A mathematical model for bone tissue regeneration inside a specific type of scaffold. Biomech Model Mechanobiol 7:355-366.

31. Prendergast PJ, Huiskes R, Søballe K. 1997. Biophysical stimuli on cells during tissue differentiation at implant interfaces. J Biomech 30:539-548.

32. Boccaccio A, Vena P, Gastaldi D, et al. 2008. Finite Element Analysis in cancellous bone failure in the vertebral body of healthy and osteoporotic subjects. Proc Inst Mech Eng H 222:1023-1036.

33. Genant HK, Wu CY, van Kuijk C, et al. 1993. Vertebral fracture assesssment using a semi-quantitative technique. J Bone Miner Res 8:1137-1148.

34. Hori RY, Lewis JL. 1982. Mechanical properties of the fibrous tissue found at the bone cement interface following total joint replacement. J Biomed Mater Res 16:911-927.

35. Armstrong CG, Mow VC. 1982. Variations in the intrinsic mechanical properties of human articular cartilage with age, degeneration and water content. J Bone Joint Surg 64A:88-94.

36. Ochoa JA, Hillberry BM. 1992. Permeability of bovine cancellous bone. Trans. of the 38th ORS, p. 162.

37. Hou FJ, Lang SM, Hoshaw SJ, et al. 1998. Human vertebral body apparent and hard tissue stiffness. J Biomech 31:1009-1015.

38. Davy D, Connoly J. 1982. The biomechanical behaviour of healing canine radii and ribs. J Biomech 15:235-247.

39. Huiskes R, van Driel WD, Prendergast PJ, et al. 1997. A biomechanical regulatory model of periprosthetic tissue differentiation. J Mater Sci Mater Med 8:785-788.

40. Boccaccio A , Pappalettere C, Kelly DJ. 2007. The influence of expansion rates on mandibular distraction osteogenesis: A computational analysis. Ann Biomed Eng 35:1940-1960.

41. Boccaccio A, Prendergast PJ, Pappalettere C, et al. 2008. Tissue differentiation and bone regeneration in an osteotomized mandible: a computational analysis of the latency period. Med Biol Eng Comput 46:283-298.

42. Rohlmann A, Zander T, Bergmann G. 2006. Spinal loads after osteoporotic vertebral fractures treated by vertebroplasty or kyphoplasty. Eur Spine J 15:1255-1264.

43. Huiskes R, Rulmerman R, Van Lenthe GH, et al. 2000. Effects of mechanical forces on maintenance and adaptation of form in trabecular bone. Nature 405:704-706.

44. McNamara LM, Prendergast PJ. 2007. Bone remodelling algorithms incorporating both strain and microdamage stimuli. J Biomech 40:1381-1391.

45. Mulvihill BM, McNamara LM, Prendergast PJ. 2008. Loss of trabeculae by mechano-biological means may explain rapid bone loss in osteoporosis. J R Soc Interface 5:1243-1253.

46. Sandino C, Planell JA, Lacroix D. 2008. A finite element study of mechanical stimuli in scaffolds for bone tissue engineering. J Biomech 41:1005-1014.

47. Kelly DJ, Prendergast PJ, 2005. Mechano-regulation of stem cell differentiation and tissue regeneration in osteochondral defects. J Biomech 38:1413-22.

48. Andreykiv A, Prendergast PJ, van Keulen F, Swieszkowski W, Rozing PM, 2005. Bone ingrowth simulation for a concept glenoid component design. J Biomech 38:1023-1033.

49. Geris L, Gerisch A, Sloten JV, et al. 2008. Angiogenesis in bone fracture healing: A bioregulatory model. J Theor Biol 251:137-158.

50. Geris L, Gerisch A, Maes C, et al. 2006. Mathematical modeling of fracture healing in mice: Comparison between experimental data and numerical simulation results. Med Biol Eng Comput 44, 280-289.

51. Bailón-Plaza A, Van Der Meulen MCH. 2001. A mathematical framework to study the effects of growth factor influences on fracture healing. J Theor Biol 212:191-209.

52. Lacroix D, Prendergast PJ, Li G, et al. 2002. Biomechanical model to simulate tissue differentiation and bone regeneration: application to fracture healing. Med Biol Eng Comput 40: 14-21.

53. Lacroix D, Prendergast PJ, 2002. Three-dimensional simulation of fracture repair in the human tibia.. Comput Methods Biomech Biomed Engin 5:369-76.

FIGURE CAPTIONS

Figure 1: Finite element models of the spinal segment L3-L4-L5; the body of vertebra L4 was modelled firstly as healthy (A), and then as fractured (B). The height of the healthy vertebra (C) was constant, the height of the fractured one (D) decreased towards the anterior side. The fracture gap was located in the centre of the vertebral body and its thickness decreased towards the posterior processes (E) (the fracture gap is highlighted in red).

Figure 2: Geometry and principal dimensions of the micro-scale model of the trabecular bone. In orange are represented the trabeculae spicules, in green the granulation tissue which was hypothesized to occupy the space between the trabeculae initially after the fracture event.

Figure 3: Points ($P_1, P_2, \ldots, P_8$) within the fracture gap where analysis of the fracture repair process was carried out.

Figure 4: Schematic of the algorithm utilized to model the fracture repair process.

Figure 5: Maps of the Von Mises stress (A) and of the u_3 displacement component field in the healthy (B) and in the fractured (C) model (first day after the fracture event).

Figure 6: Patterns of the tissues differentiating during the fracture healing process in the point P_1.

Figure 7: Patterns of the bony tissue forming during the fracture healing process in the points P_1, P_2, and P_3.

Figure 8: Percentages of tissues differentiating during the healing process in the points P_1 (A), P_2 (B) and P_3 (C). The percentages of tissues within the fractured region have been computed by dividing the number of elements of a given tissue by the total number of elements making up the micro-scale model. 'Resorption' indicates the number of elements for which $S<0.01$. The space originally occupied by the trabeculae before the fracture is 1/4 (25%) of the total available space.

TABLES

Table 1
Material properties utilized in the micro-scale model for the trabecular bone and the fractured region.[14,34-37]

Material	Granulation tissue	Fibrous tissue	Cartilage	Mature Bone	Trabeculae spicules
Young's Modulus [MPa]	0.2	2	10	1440	4400
Permeability [m^4/Ns]	$1*10^{-14}$	$1*10^{-14}$	$5*10^{-15}$	$3.7*10^{-13}$	$1\cdot10^{-17}$
Poisson's Ratio	0.167	0.167	0.167	0.3	0.3

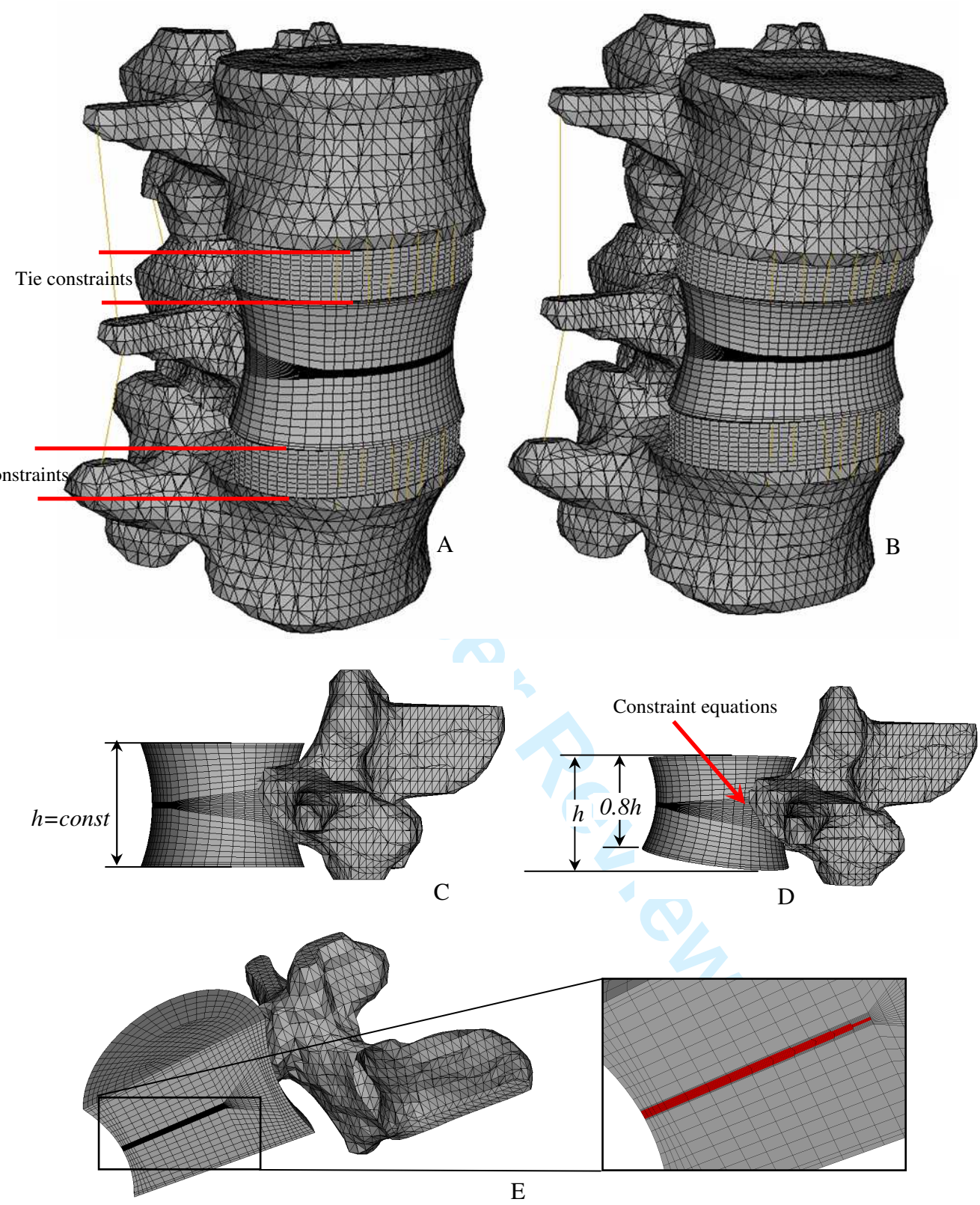

Figure 1: Finite element models of the spinal segment L3-L4-L5; the body of vertebra L4 was modelled firstly as healthy (A), and then as fractured (B). The height of the healthy vertebra (C) was constant, the height of the fractured one (D) decreased towards the anterior side. The fracture gap was located in the centre of the vertebral body and its thickness decreased towards the posterior processes (E) (the fracture gap is highlighted in red).

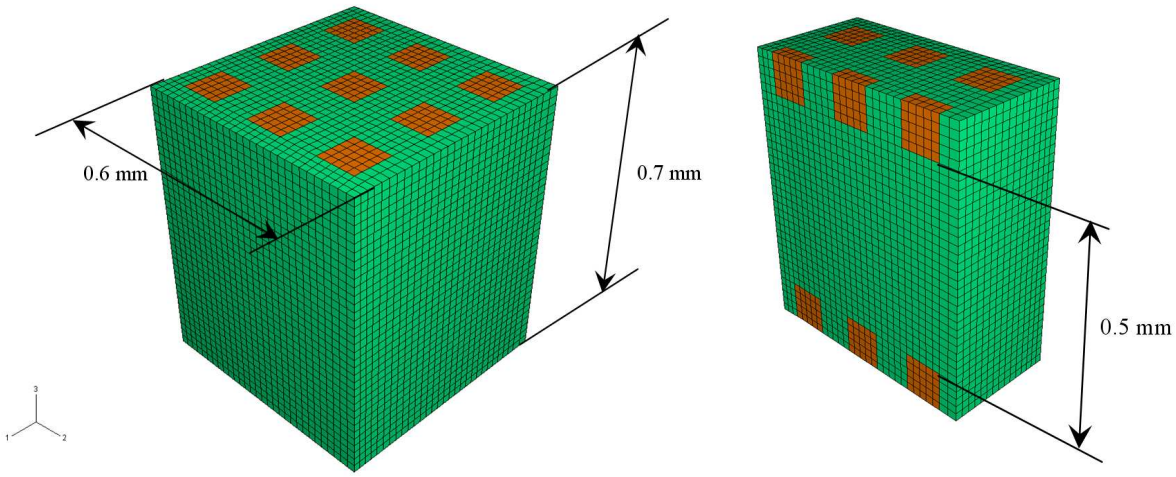

Figure 2: Geometry and principal dimensions of the micro-scale model of the trabecular bone. In orange are represented the trabeculae spicules, in green the granulation tissue which was hypothesized to occupy the space between the trabeculae initially after the fracture event.

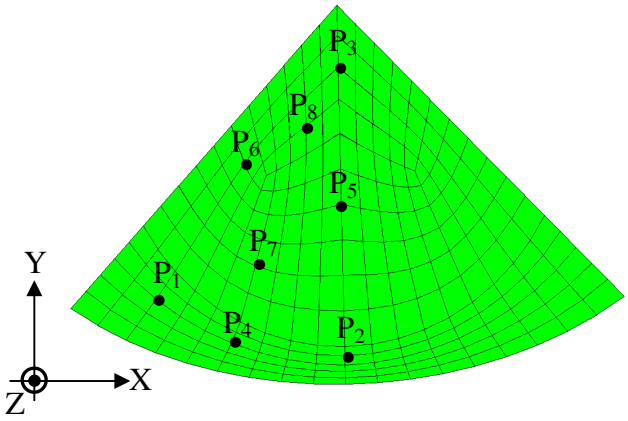

Figure 3: Points (P_1, P_2,…, P_8) within the fracture gap where analysis of the fracture repair process was carried out.

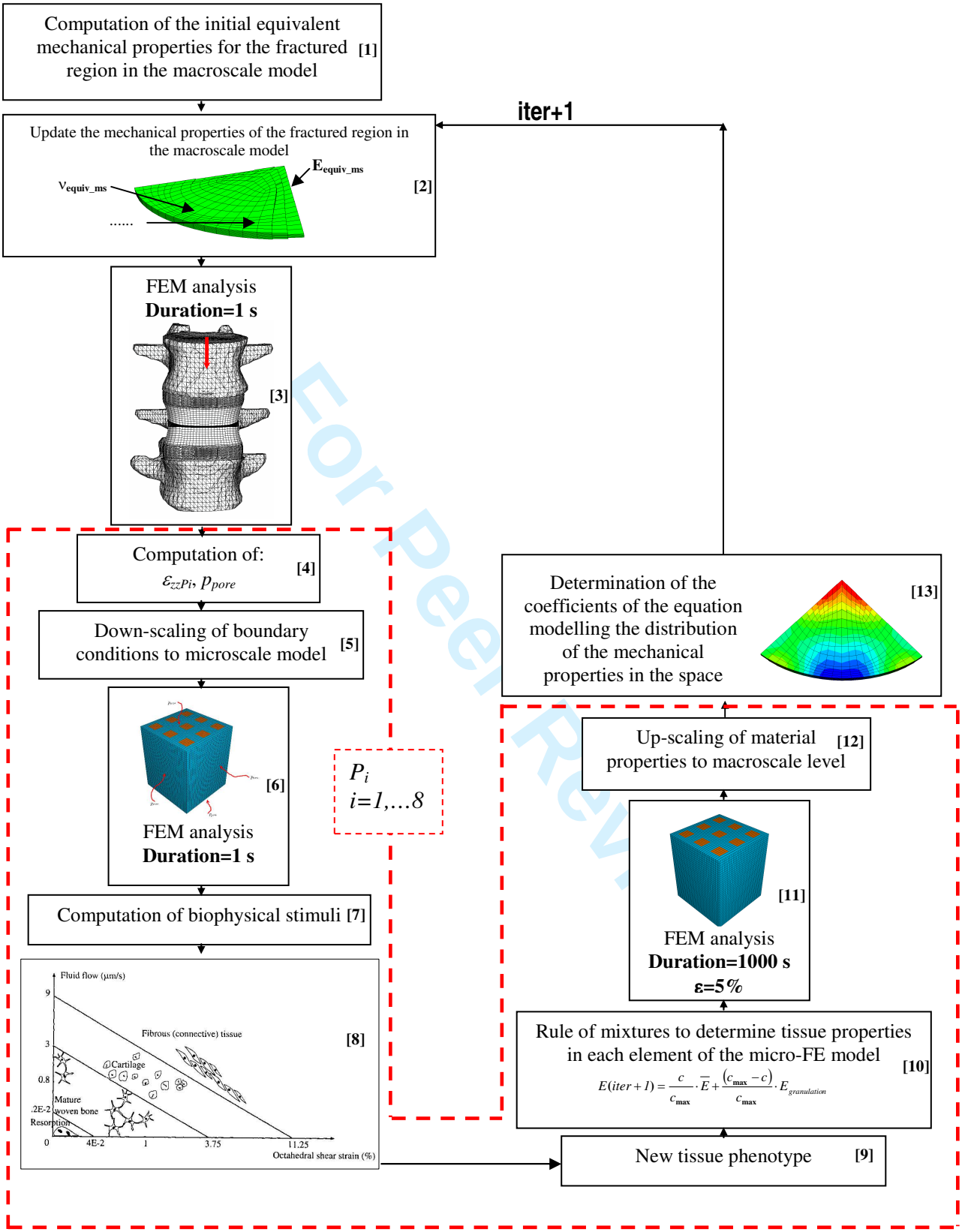

Figure 4: Schematic of the algorithm utilized to model the fracture repair process.

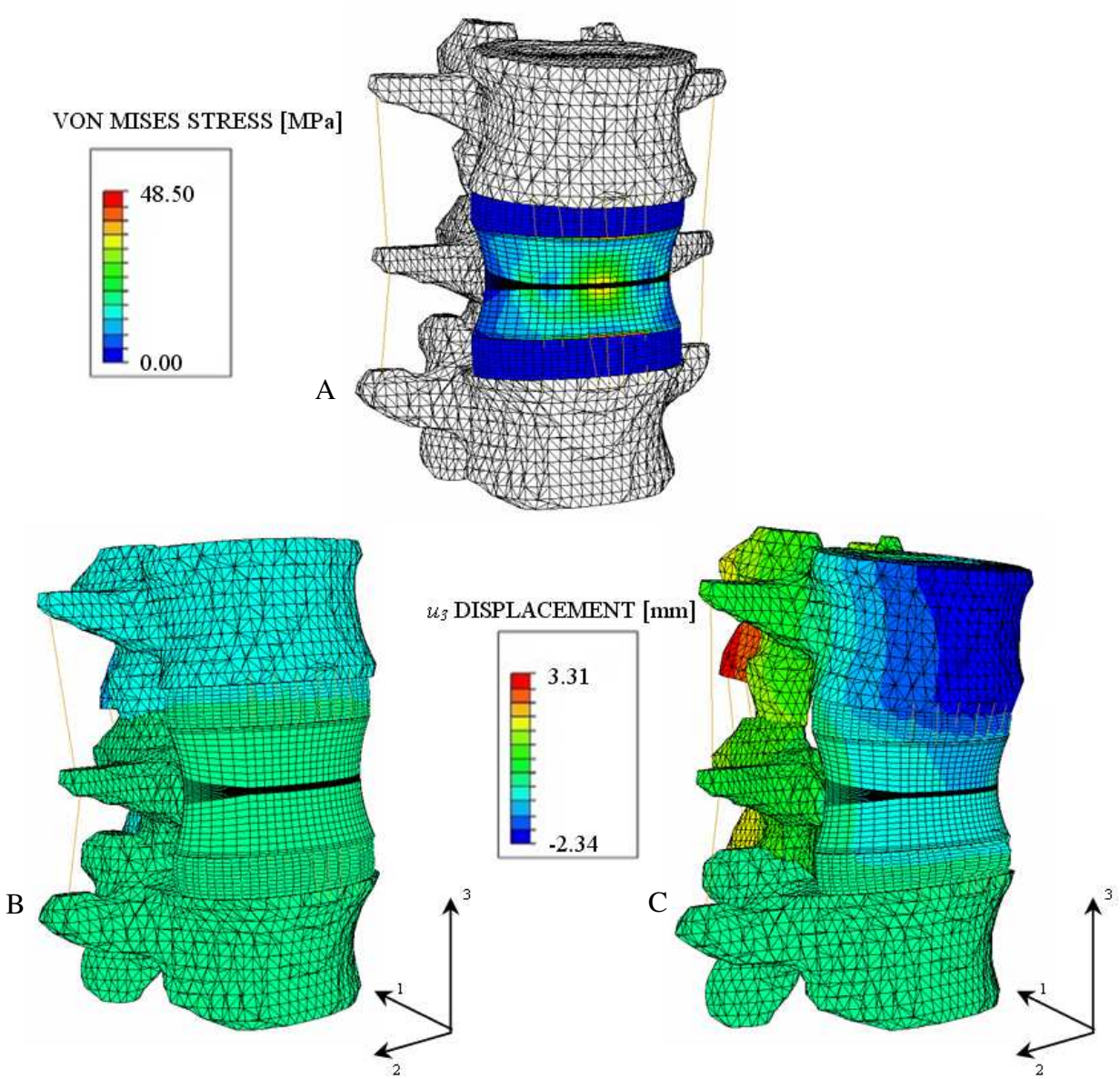

Figure 5: Maps of the Von Mises stress (A) and of the u_3 displacement component field in the healthy (B) and in the fractured (C) model (first day after the fracture event).

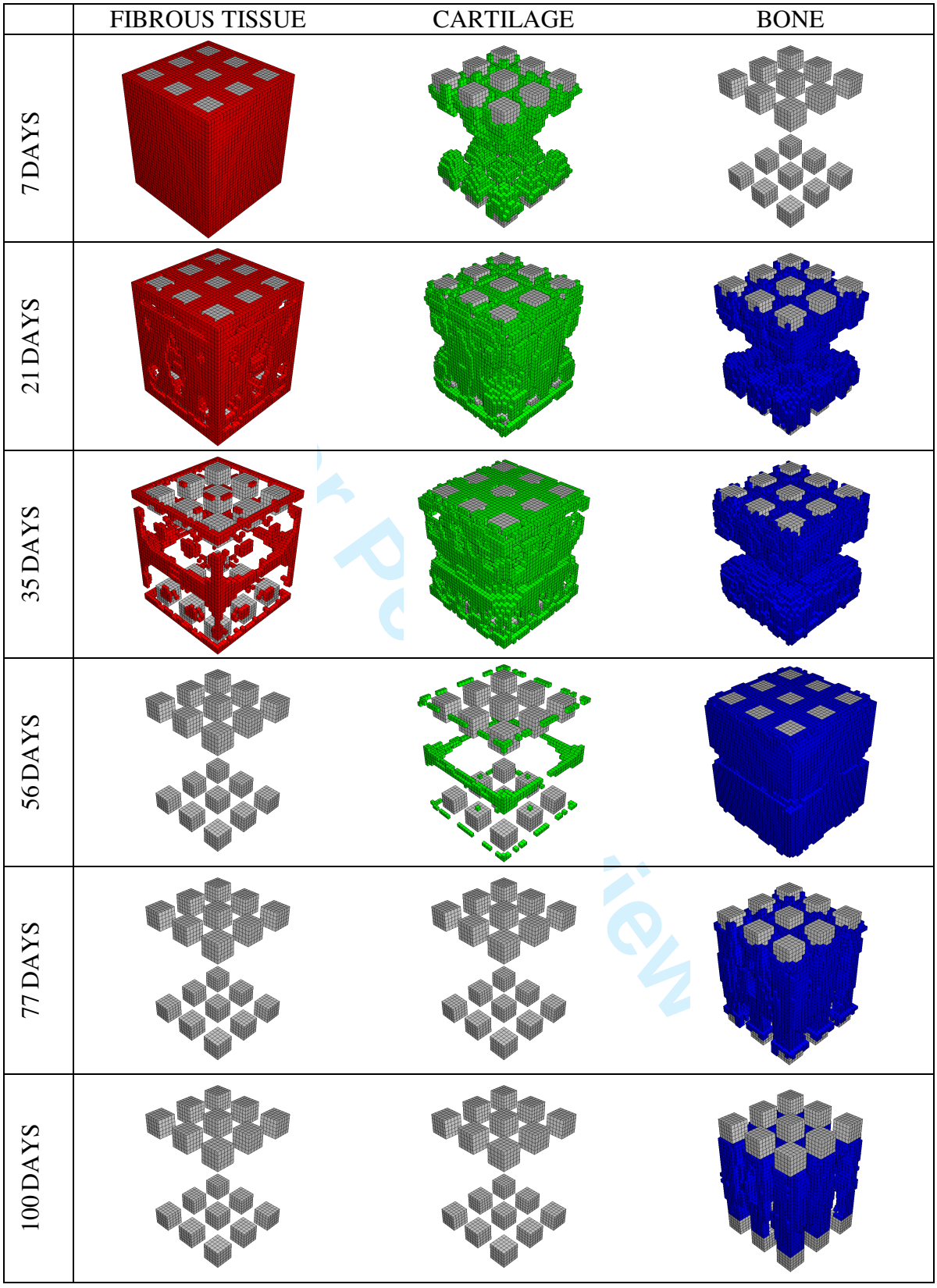

Figure 6: Patterns of the tissues differentiating during the fracture healing process in the point P_1.

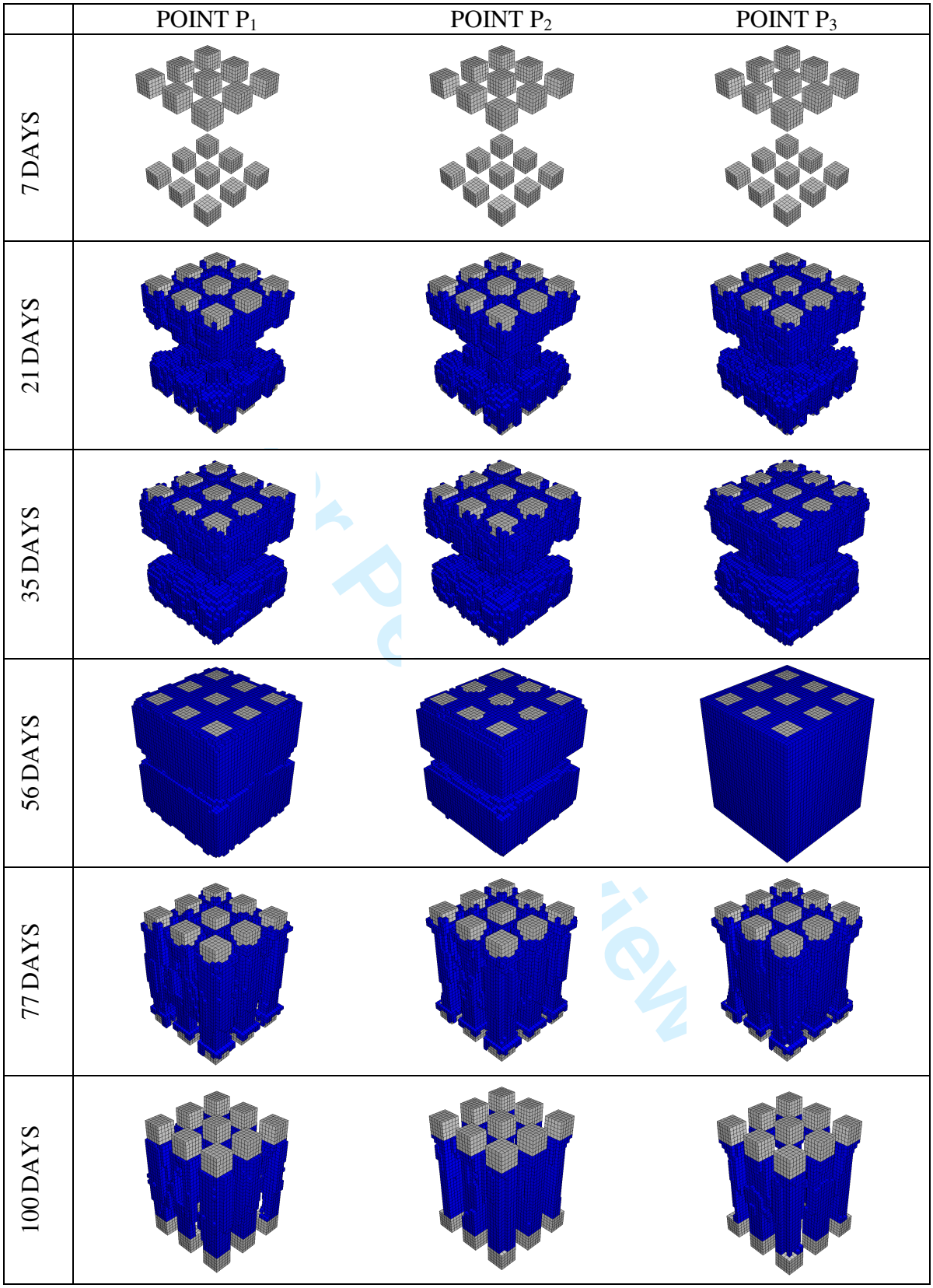

Figure 7: Patterns of the bony tissue forming during the fracture healing process in the points P_1, P_2, and P_3.

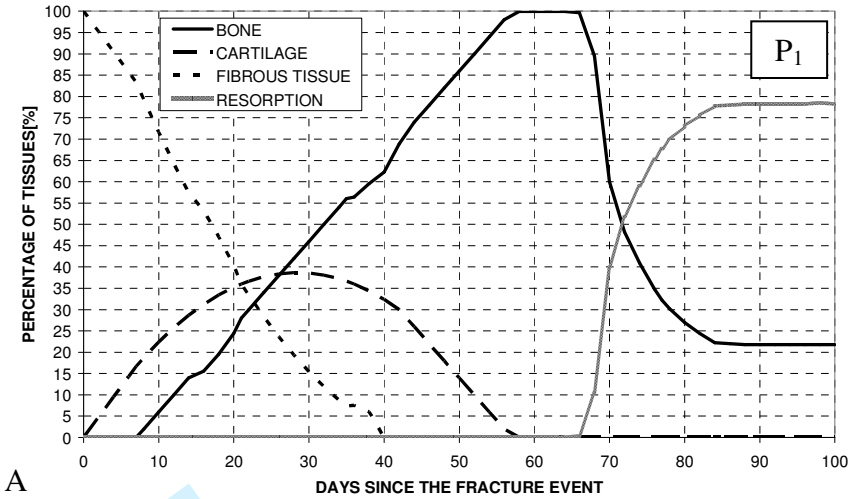

A

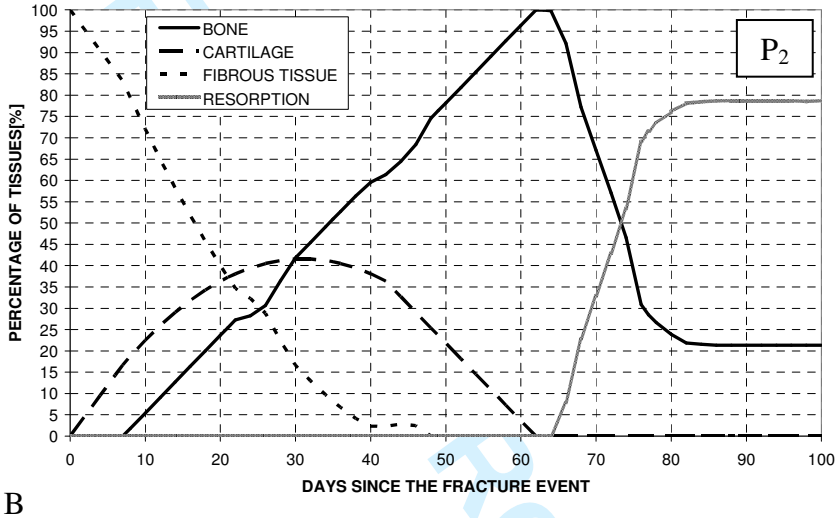

B

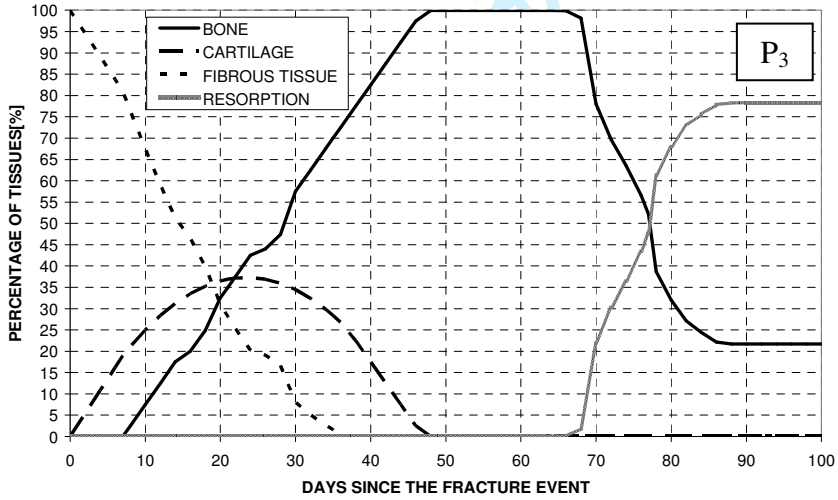

C

Figure 8: Percentages of tissues differentiating during the healing process in the points P_1 (A), P_2 (B) and P_3 (C). The percentages of tissues within the fracture gap have been computed by dividing the number of elements of a given tissue by the total number of elements making up the micro-scale model. 'Resorption' indicates the number of elements for which $S<0.01$. The space originally occupied by the trabeculae before the fracture is 1/4 (25%) of the total available space.